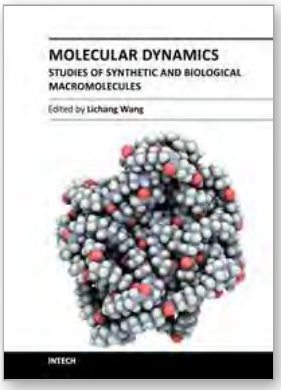

Molecular Dynamics - Studies of Synthetic and Biological Macromolecules

Edited by Prof. Lichang Wang

ISBN 978-953-51-0444-5
Hard cover, 432 pages
Publisher InTech
Published online 11, April, 2012
Published in print edition April, 2012

Molecular Dynamics is a two-volume compendium of the ever-growing applications of molecular dynamics simulations to solve a wider range of scientific and engineering challenges. The contents illustrate the rapid progress on molecular dynamics simulations in many fields of science and technology, such as nanotechnology, energy research, and biology, due to the advances of new dynamics theories and the extraordinary power of today's computers. This second book begins with an introduction of molecular dynamics simulations to macromolecules and then illustrates the computer experiments using molecular dynamics simulations in the studies of synthetic and biological macromolecules, plasmas, and nanomachines. Coverage of this book includes: Complex formation and dynamics of polymers Dynamics of lipid bilayers, peptides, DNA, RNA, and proteins Complex liquids and plasmas Dynamics of molecules on surfaces Nanofluidics and nanomachines

How to reference

In order to correctly reference this scholarly work, feel free to copy and paste the following:

Martin Oliver Steinhauser (2012). Introduction to Molecular Dynamics Simulations: Applications in Hard and Soft Condensed Matter Physics, Molecular Dynamics - Studies of Synthetic and Biological Macromolecules, Prof. Lichang Wang (Ed.), ISBN: 978-953-51-0444-5, InTech, Available from: http://www.intechopen.com/books/molecular-dynamics-studies-of-synthetic-and-biological-macromolecules/introduction-to-molecular-dynamics-simulations-applications-in-hard-and-soft-condensed-matter-physic

INTECH
open science | open minds

InTech Europe
University Campus STeP Ri
Slavka Krautzeka 83/A
51000 Rijeka, Croatia
Phone: +385 (51) 770 447
Fax: +385 (51) 686 166
www.intechopen.com

InTech China
Unit 405, Office Block, Hotel Equatorial Shanghai
No.65, Yan An Road (West), Shanghai, 200040, China
中国上海市延安西路65号上海国际贵都大饭店办公楼405单元
Phone: +86-21-62489820
Fax: +86-21-62489821

1

Introduction to Molecular Dynamics Simulations: Applications in Hard and Soft Condensed Matter Physics

Martin Oliver Steinhauser
Research Group Shock Waves in Soft Biological Matter, Department of Composite Materials
Fraunhofer Institute for High-Speed Dynamics, Ernst-Mach-Institut, EMI, Eckerstrasse 4, Freiburg
Germany

1. Introduction

Today, computer experiments play a very important role in science. In the past, physical sciences were characterized by an interplay between experiment and theory. In theory, a model of the system is constructed, usually in the form of a set of mathematical equations. This model is then validated by its ability to describe the system behavior in a few selected cases, simple enough to allow a solution to be computed from the equations. One might wonder why one does not simply derive all physical behavior of matter from an as small as possible set of fundamental equations, e.g. the Dirac equation of relativistic quantum theory. However, the quest for the fundamental principles of physics is not yet finished; thus, the appropriate starting point for such a strategy still remains unclear. But even if we knew all fundamental laws of nature, there is another reason, why this strategy does not work for ultimately predicting the behavior of matter on any length scale, and this reason is the growing complexity of fundamental theories – which are based on the dynamics of particles – when they are applied to systems of macroscopic (or even microscopic) dimensions. In almost all cases, even for academic problems involving only a few particles[1], a strict analytical solution is not possible and solving the problem very often implies a considerable amount of simplification. In contrast to this, in experiments, a system is subject to measurements, and results are collected, very often in the form of large data sets of numbers from which one strives to find mathematical equations describing the data by generalization, imagination and by thorough investigation. Very rarely, normally based on symmetries which allow inherent simplifications of the original problem, is an analytical solution at hand which describes exactly the evidence of the experiment given by the obtained data sets. Unfortunately, many academic and practical physical problems of interest do not fall under this category of "simple" problems, e.g. disordered systems, where there is no symmetry which helps to simplify the treatment.

The advent of modern computers which basically arose from the Manhattan project in the United States in the 1950s added another element to (classical) experiment and theory, namely

[1] In fact, already the three-body problem which involves three coupled ordinary differential equations is not solvable analytically.

the *computer experiment*. Some traditionalists working in theory, who have not followed the modern developments of computer science and its applications in the realm of physics, biology, chemistry and many more scientific fields, still repudiate the term "experiment" in the context of computer simulations. However, this term is most certainly fully justified!

In a computer experiment, a model is still provided by theory, but the calculations are carried out by the machine by following a series of instructions (the *algorithm*) usually coded in some high-level language and translated (*compiled*) into assembler commands which provide instructions how to manipulate the contents of processor registers. The results of computer simulations are just numbers, data which have to be interpreted by humans, either in the form of graphical output, as tables or as function plots. By using a machine to carry out the calculations necessary for solving a model, more complexity can be introduced and more realistic systems can be investigated.

Simulation is seen sometimes as theory, sometimes as experiment. On the one side, one is still dealing with models, not with "real systems"[2] On the other side, the procedure of verifying a model by computer simulation resembles an experiment very closely: One performs a run, then analyzes the results in pretty much the same way as an experimental physicist does. Simulations can come very close to experimental conditions which allows for interpreting and understanding the experiments at the microscopic level, but also for studying regions of systems which are not accessible in "real" experiments[3], too expensive to perform, or too dangerous. In addition, computer simulations allow for performing *thought experiments*, which are impossible to do in reality, but whose outcome greatly increases our understanding of fundamental processes or phenomena. Imagination and creativity, just like in mathematics[4], physics and other scientific areas, are very important qualities of a computer simulator!

From a principal point of view, theory is traditionally based on the reductionist approach: one deals with complexity by reducing a system to simpler subsystems, continuing until the subsystems are simple enough to be represented with solvable models. From this perspective one can regard simulation as a convenient tool to verify and test theories and the models associated with them in situations which are too complex to be handled analytically[5]. Here, one implies that the model represents the level of the theory where the interest is focused.

However, it is important to notice that simulation can play a more important role than just being a tool to be used as an aid to reductionism because it can be considered as an *alternative* to it. Simulation increases considerably the threshold of complexity which separates solvable und unsolvable models. One can take advantage of this threshold shift and move up several levels in our description of physical systems. Thanks to the presence of simulation, we do not need to work with models as simple as those used in the past. This gives the researcher an additional freedom for exploration. As an example, one could mention the interatomic potentials which, in the past, were obtained by two-body potentials with simple

[2] In this context one has to realize that often, in experiments, too, considerable simplifications of the investigated "real system" are done, e.g. when preparing it in a particular state in terms of pressure, temperature or other degrees of freedom.
[3] For example, systems at a pressure comparable to that in the interior of the sun.
[4] The famous David Hilbert once commented the question of what became of one of his students: "He became a writer - he didn't have enough imagination."
[5] For example, when computing the phase diagram of a substance modeled by a certain force law.

analytical form, such as Morse or Lennard-Jones. Today, the most accurate potentials contain many-body terms and are determined numerically by reproducing as closely as possible the forces predicted by ab-initio methods. These new potentials could not exist without simulation, so simulation is not only a connecting link between theory and experiment, but it is also a powerful tool to make progress in new directions. Readers, interested in these more "philosophical" aspects of computational science will be able to find appropriate discussions in the first chapters of refs. (Haile, 1992; Steinhauser, 2008; 2012). In the following, we focus on *classical* molecular dynamics (MD) simulations, i.e. a variant of MD which neglects any wave character of discrete atomic particles, describing them as classical in the Newtonian sense and not referring to any quantum mechanical considerations.

2. The objective of molecular dynamics simulations

Molecular dynamics computer experiments are done in an attempt of understanding the properties of assemblies of molecules in terms of their structure and the microscopic interactions between them. We provide a guess at the interactions between molecules, and obtain exact predictions of bulk properties. The predictions are "exact" in the sense that they can be made as accurate as we like, subject to the limitations imposed by our computer budget. At the same time, the hidden dynamic details behind bulk measurements can be revealed. An example is the link between the diffusion coefficient and the velocity autocorrelation function, with the latter being very hard to measure experimentally, but the former being very easy to measure. Ultimately one wants to make direct comparison with experimental measurements made on specific materials, in which case a good model of molecular interactions is essential. The aim of so-called ab-inito MD is to reduce the amount of guesswork and fitting in this process to a minimum. On the other hand, sometimes one is merely interested in phenomena of a rather generic nature, or one wants to discriminate between bad and good theories. In this case it is not necessary to have a perfectly realistic molecular model, but one that contains the essential physics may be quite suitable.

2.1 Molecular interactions

Classical MD simulation consists of the numerical, step-by-step solution of the classical Newtonian equations of motion, which for a simple atomic system may be written as

$$m_i \ddot{\vec{r}}_i = \vec{F}_i = -\frac{\partial}{\partial \vec{r}_i}\Phi, \tag{1}$$

where the vector symbol in the partial derivative is a physicsts' abbreviatory notation for the derivate of each individual component. To solve Eq. 1 one needs to calculate the forces $\vec{F}_i$ acting on the atoms, which are usually derived from a potential energy function $\Phi(\vec{r}^N)$, where $\vec{r}^N = (\vec{r}_1, \vec{r}_2, ..., \vec{r}_N)$ represents the complete set of $3N$ atomic coordinates.

2.1.1 Bonded interactions

Using the notion of intermolecular potentials acting between the particles of a system one cannot only model fluids made of simple spherically symmetric particles but also more complex molecules with internal degrees of freedom (due to their specific monomer connectivity). If one intends to incorporate all aspects of the chemical bond in complex molecules one has to treat the system with quantum chemical methods. Usually, one

considers the internal degrees of freedom of polymers and biomacromolecules by using generic potentials that describe bond lengths l_i, bond angles θ and torsion angles ϕ. When neglecting the fast electronic degrees of freedom, often bond angles and bond lengths can be assumed to be constants. In this case, the potential includes lengths l_0 and angles θ_0, ϕ_0 at equilibrium about which the molecules are allowed to oscillate, and restoring forces which ensure that the system attains these equilibrium values on average. Hence the bonded interactions Φ_{bonded} for polymeric macromolecular systems with internal degrees of freedom can be treated by using some or all parts of the following potential term:

$$\Phi_{bonded}(r,\theta,\phi) = \frac{\kappa}{2}\sum_i (\mid \vec{r}_i - \vec{r}_{i-1} - l_0 \mid)^2 + \frac{k_\theta}{2}\sum_k (\theta_k - \theta_0)^2 + \frac{\beta}{2}\sum_m (\phi_m - \phi_0)^2. \quad (2)$$

Here, the summation indices sum up the number of bonds i at positions $\vec{r}_i$, the number of bond angles k between consecutive monomers along a macromolecular chain and the number of torsion angles m along the polymer chain. A typical value of $\kappa = 5000$ ensures that the fluctuations of bond angles are very small (below 1%). The terms l_0, θ_0 and ϕ_0 are the equilibrium distance, bond angle and torsion angle, respectively.

In particular in polymer physics, very often a Finitely Extensible Non-linear Elastic (FENE) potential is used which - in contrast to a harmonic potential - restricts the maximum bond length of a polymer bond to a prefixed value R_0 (Steinhauser, 2005):

$$\Phi_{FENE}(r) = \begin{cases} -\frac{1}{2}\kappa R_0^2 \ln(1 - \frac{r^2}{R_0^2}) & r < R_0, \\ \infty & \text{otherwise.} \end{cases} \quad (3)$$

The FENE potential can be used instead of the first term on the right hand side of the bonded potential in Eq. 2. Figure 1 illustrates the different parameters which are used in the description of bonded interactions in Eq. 2. Further details on the use of potentials in macromolecular biology and polymer physics may be found in (Feller, 2000; Schlenkrich et al., 1996; Siu et al., 2008; Steinhauser, 2008).

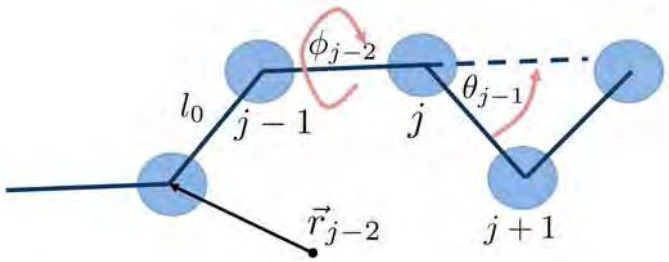

Fig. 1. Illustration of the potential parameters used for modeling bonded interactions.

2.1.2 Non-bonded interactions

Various physical properties are determined by different regions of the potential hypersurface of interacting particles. Thus, for a complete determination of potential curves, widespread experiments are necessary. For a $N-$body system the total energy Φ_{nb}, i.e. the potential

hypersurface of the non-bonded interactions can be written as (Allen & Tildesly, 1991)

$$\Phi_{nb}(\vec{r}) = \sum_{i}^{N} \phi_1(\vec{r}_i) + \sum_{i}^{N}\sum_{j>i}^{N} \phi_2(\vec{r}_i,\vec{r}_j) + \sum_{i}^{N}\sum_{j>i}^{N}\sum_{k>j>i}^{N} \phi_3(\vec{r}_i,\vec{r}_j,\vec{r}_k) + \cdots, \tag{4}$$

where $\phi_1, \phi_2, \phi_3, \ldots$ are the interaction contributions due to external fields (e.g. the effect of container walls) and due to pair, triple and higher order interactions of particles. In classical MD one often simplifies the potential by the hypothesis that all interactions can be described by pairwise additive potentials. Despite this reduction of complexity, the efficiency of a MD algorithm taking into account only pair interactions of particles is rather low (of order $\mathcal{O}(N^2)$) and several optimization techniques are needed in order to improve the runtime behavior to $\mathcal{O}(N)$.

The simplest general Ansatz for a non-bonded potential for spherically symmetric systems, i.e. $\Phi(\vec{r}) = \Phi(r)$ with $r = |\vec{r}_i - \vec{r}_j|$ is a potential of the following form:

$$\Phi_{nb}(r) = \Phi_{Coulomb}(r) + \left(\frac{C_1}{r}\right)^{12} + \left(\frac{C_2}{r}\right)^{6}. \tag{5}$$

Parameters C_1 and C_2 are parameters of the attractive and repulsive interaction and the electrostatic energy $\Phi_{Coulomb}(r)$ between the particles with position vectors $\vec{r}_i$ and $\vec{r}_j$ is given by:

$$\Phi_{Coulomb}(r) = \frac{1}{\epsilon} k \cdot \sum_{i}\sum_{j>i} \frac{z_i z_j e^2}{|\vec{r}_i - \vec{r}_j|}. \tag{6}$$

The constant $k = 1$ in the cgs–system of units and ϵ is the dielectric constant of the medium, for example $\epsilon_{air} = 1$ for air, $\epsilon_{prot} = 4$ for proteins or $\epsilon_{H_20} = 82$ for water. The variables z_i and z_j denote the charge of individual monomers in the macromolecule and e is the electric charge of an electron.

The probably most commonly used form of the potential of two neutral atoms which are only bound by Van-der-Waals interactions, is the *Lennard-Jones (LJ), or (a-b) potential* which has the form (Haberland et al., 1995)

$$\Phi_{a,b}(r) = \alpha\varepsilon \left[\left(\frac{\sigma_0}{r}\right)^{a} + \left(\frac{\sigma_0}{r}\right)^{b} \right], \tag{7}$$

where

$$\alpha = \frac{1}{a-b}\left(\frac{a^a}{b^b}\right)^{\frac{1}{a-b}}, \ \Phi_{\min} = \varepsilon \text{ and } \Phi(\sigma) = 0. \tag{8}$$

The most often used LJ-(6-12) potential for the interaction between two particles with a distance $r = |\vec{r}_i - \vec{r}_j|$ then reads (cf. Eq. 5):

$$\Phi_{LJ}(r) = 4\varepsilon \left[\left(\frac{\sigma_0}{r}\right)^{12} + \left(\frac{\sigma_0}{r}\right)^{6} \right]. \tag{9}$$

Parameter ε determines the energy scale and σ_0 the length scale. In simulations one uses dimensionless *reduced units* which tend to avoid numerical errors when processing very small numbers, arising e.g. from physical constants such as the Boltzmann constant $k_B = 1.38 \times$

10^{-23}J/K. In these reduced (simulation) units, one MD timestep is measured in units of $\hat{\tau} = (m\sigma^2/\varepsilon)^{1/2}$, where m is the mass of a particle and ε and σ_0 are often simply set to $\sigma_0 = \varepsilon = k_B T = 1$. Applied to real molecules, for example to Argon with $m = 6.63 \times 10^{-23} kg, \sigma_0 \approx 3.4 \times 10^{-10} m$ and $\varepsilon/k_B \approx 120K$ one obtains a typical MD timestep of $\hat{\tau} \approx 3.1 \times 10^{-13} s$.

Using an exponential function instead of the repulsive r^{-12} term, one obtains the *Buckingham potential* (Buckingham, 1938):

$$\Phi(r) = b \exp(-ar) - \frac{c}{r^6} - \frac{d}{r^8}. \tag{10}$$

This potential however has the disadvantage of using a numerically very expensive exponential function and it is known to be unrealistic for many substances at small distances r where it has to be modified accordingly.

For reasons of efficiency, a classical MD potential should be short-ranged in order to keep the number of force calculations between interacting particles at a minimum. Therefore, instead of using the original form of the potential in Eq. 9, which approaches 0 at infinity, it is common to use a modified form, where the potential is simply cut off at its minimum value $r = r_{\min} = \sqrt[6]{2}$ and shifted to positive values by ε such that it is purely repulsive and smooth at $r = r_{\text{cut}} = \sqrt[6]{2}$:

$$\Phi_{LJ}^{\text{cut}}(r) = \begin{cases} 4\,\varepsilon \left\{ \left(\frac{\sigma_0}{r}\right)^{12} - \left(\frac{\sigma_0}{r}\right)^{6} \right\} + \varepsilon & r \leq 2^{1/6}\sigma_0, \\ 0 & \text{otherwise.} \end{cases} \tag{11}$$

Another extension of the potential in Eq. 9 is proposed in (Steinhauser, 2005) where a smooth attractive part is introduced again, in order to allow for including different solvent qualities of the solvent surrounding the polymer:

$$\Phi_{cos}(r) = \left[\frac{1}{2} \cdot \cos(\alpha r^2 + \beta) + \gamma \right] \varepsilon. \tag{12}$$

This additional term adds an attractive part to the potential of Eq. 11 and at the same time – by appropriately choosing parameters α, β and γ – keeps the potential cutoff at r_{cut} smooth. The parameters α, β and γ are determined analytically such that the potential tail of Φ_{cos} has zero derivative at $r = 2^{1/6}$ and at $r = r_{\text{cut}}$, while it is zero at $r = r_{\text{cut}}$ and has value γ at $r = 2^{1/6}$, where γ is the depth of the attractive part. Further details can be found in (Steinhauser, 2005). When setting $r_{\text{cut}} = 1.5$ one sets $\gamma = -$ and obtains α and β as solutions of the linear set of equations

$$2^{1/3}\alpha + \beta = \pi, \tag{13}$$

$$2.25\alpha + \beta = 2\pi. \tag{14}$$

The total unbounded potential can then be written as:

$$\Phi_{Total}(r, \lambda) = \begin{cases} \Phi_{LJ}^{\text{cut}}(r) - \lambda\varepsilon & 0 < r < 2^{1/6}\,\sigma_0, \\ \lambda\,\Phi_{cos}(r) & 2^{1/6}\,\sigma_0 \leq r < r_{\text{cut}}, \\ \infty & \text{otherwise,} \end{cases} \tag{15}$$

where λ is a new parameter of the potential which determines the depth of the attractive part. Instead of varying the solvent quality in the simulation by changing temperature T directly (and having to equilibrate the particle velocities accordingly), one can achieve a phase transition in polymer behavior by changing λ accordingly, cf. Fig. 2.

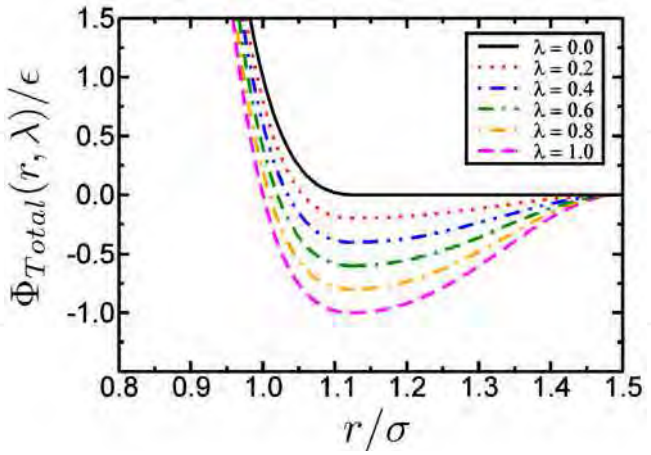

Fig. 2. Graph of the total unbounded potential of Eq. 15 which allows for modeling the effects of different solvent qualities.

Using coarse-grained models in the context of lipids and proteins, where each amino acid of the protein is represented by two coarse-grained beads, it has become possible to simulate lipoprotein assemblies and protein-lipid complexes for several microseconds (Shih et al., 2006).

The assumption of a short ranged interaction is usually fulfilled very well for all (uncharged) polymeric fluids. However, as soon as charged systems are involved this assumption breaks down and the calculation of the Coulomb force requires special numerical treatment due to its infinite range.

2.2 Calculation of forces

The most crucial part of a MD simulation is the force calculation. At least 95% of a MD code is spent with the force calculation routine which uses a search algorithm that determines interacting particle pairs. Therefore this is the task of a MD program which has to be optimized first and foremost. We will review a few techniques that have become standard in MD simulations which enhance the speed of force calculations considerably and speed up the algorithm from $\mathcal{O}(N^2)$ run time to $\mathcal{O}(N)$ run time. Starting from the original LJ potential between two particles i and j with distance $r = |\vec{r}_i - \vec{r}_j|$ of Eq. 7, one obtains the potential function for N interacting particles as the following double sum over all particles:

$$\Phi(\vec{r}_1,...,\vec{r}_N) = \sum_{i=1}^{N}\sum_{j=i+1}^{N} \Phi_{LJ}(r) = 4\varepsilon \sum_{i=1}^{N}\sum_{j=i+1}^{N} \left(\frac{\sigma_0}{r}\right)^6 \times \left(\left(\frac{\sigma_0}{r}\right)^6 - 1\right). \tag{16}$$

The corresponding force $\vec{F}_i$ exerted on particle i by particle j is given by the gradient with respect to $\vec{r}_i$ as:

$$\vec{F}_i = -\nabla_{\vec{r}_i}\Phi_{LJ}(\vec{r}_1,...,\vec{r}_N) = -24\times\varepsilon\sum_{j=1,j\neq i}^{N}\frac{1}{r^2}\times\left(\frac{\sigma_0}{r}\right)^6\times\left(1-2\times\left(\frac{\sigma_0}{r}\right)^6\right)\vec{r}_{ij}, \quad (17)$$

where $\vec{r}_{ij} = (\vec{r}_i - \vec{r}_j)$ is the direction vector between particles i and j at positions $\vec{r}_i$ and $\vec{r}_j$, and $r = |\vec{r}_i - \vec{r}_j|$. Hence, in general, the force $\vec{F}_i$ on particle i is the sum over all forces $\vec{F}_{ij} := -\nabla_{\vec{r}_i}\Phi$ between particle i and all other particles j:

$$\vec{F}_i = \sum_{i=1,j\neq i}^{N}\vec{F}_{ij}. \quad (18)$$

The least favorable method of looking for interacting pairs of particles and for calculating the double sum in Eqs. 16 and 17 is the "brute force" method that simply involves taking a double loop over all particles in the (usually) cubic simulation box, thus calculating $\frac{1}{2}N(N-1)$ interactions with a N^2 efficiency. This algorithm becomes extremely inefficient for systems of more than a few thousand particles, cf. Fig. 3(a).

2.3 The MD algorithm

The last decade has seen a rapid development in our understanding of numerical algorithms which have been summarized in a recent book (Steinhauser, 2008) that presents the current state of the field.

When introducing an N-dimensional position vector $\vec{r}^N = (\vec{r}_1,\vec{r}_2,...,\vec{r}_N)$, the potential energy $\Phi(\vec{r}^N)$ and the momenta $\vec{p}^N = (\vec{p}_1,\vec{p}_2,...,\vec{p}_N)$, in terms of which the kinetic energy may be written as $K(\vec{p}^N)$, then the total energy H of a classical conservative system is given by $H = \Phi + K$. The equations of motion determining all dynamics of the particles can be written as

$$\vec{r}_i = \vec{p}_i/m_i \quad and \quad \vec{p}_i = \vec{F}_i. \quad (19)$$

This is a system of coupled ordinary differential equations. Many methods exist to solve this set of equations numerically, among which the so-called *velcity Verlet-algorithm* is the one that is the most used. This algorithm integrates the equations of motion by performing the following four steps, where $\vec{r}_i$, $\vec{v}_i$, $\vec{a}_i = \vec{T}_i/m_i$ are the position, velocity and acceleration of the i-th particle, respectively:

$$\text{Calculate } \vec{v}_i(t+\frac{1}{2}\delta t) = \vec{v}_i(t) + \frac{1}{2}\delta t\vec{F}_i(t), \quad (20)$$

$$\text{Calculate } \vec{r}_i(t+\delta t) = \vec{r}_i(t) + \delta t\vec{v}_i(t+\frac{1}{2}\delta t), \quad (21)$$

$$\text{Derive } \vec{a}_i(t+\delta t) \quad \text{from the interaction potential using } \vec{r}(t+\delta t), \quad (22)$$

$$\text{Calculate } \vec{v}_i(t+\delta t) = \vec{v}_i(t+\frac{1}{2}\delta t) + +\frac{1}{2}\delta t\vec{a}_i(t+\delta t). \quad (23)$$

Further details about this standard algorithm can be found elsewhere (Steinhauser, 2008). It is exactly time reversible, symplectic, low order in time (hence permitting large timesteps), and it requires only one expensive force calculation per timestep.

2.3.1 Neighbor lists

In general, in molecular systems, the potential as well as the corresponding force decays very fast with the distance r between the particles. Thus, for reasons of efficiency, in molecular simulations one often uses the modified LJ potential of Eq. 11 which introduces a cutoff r_{cut} for the potential. The idea here is to neglect all contributions in the sums in Eqs. 16 and 17 that are smaller than the threshold r_{cut} which characterizes the range of the interaction. Thus, in this case the force $\vec{F}_i$ on particle i is approximated by

$$\vec{F}_i \approx -24 \times \varepsilon \sum_{\substack{j=1, j\neq i \\ 0<r\leq r_{\text{cut}}}}^{N} \frac{1}{r^2} \times \left(\frac{\sigma_0}{r}\right)^6 \times \left(1 - 2 \times \left(\frac{\sigma_0}{r}\right)^6\right) \vec{r}_{ij}. \tag{24}$$

Contributions to the force on particle i that stem from particles j with $r \leq r_{\text{cut}}$ are neglected. This introduces a small error in the computation of the forces and the total energy of the system, but it reduces the overall computational effort from $\mathcal{O}(N^2)$ to $\mathcal{O}(N)$. For systems with short-ranged or rapidly decaying potentials, a very efficient algorithm for the search of potentially interacting particles, i.e. those particles that are within the cutoff distance r_{cut} of a particle i, has been developed (Hockney, 1970). In MD this algorithm can be implemented most efficiently by geometrically dividing the volume of the (usually cubic) simulation box into small cubic cells whose sizes are slightly larger than the interaction range r_{cut} of particles, cf. Fig. 3b. The particles are then sorted into these cells using the linked-cell algorithm (LCA). The LCA owes its name to the way in which the particle data are arranged in computer memory, namely as linked list for each cell. For the calculation of the interactions it is then sufficient to calculate the distances between particles in neighboring cells only, since cells which are further than one cell apart are by construction beyond the interaction range. Thus, the number of distance calculations is restricted to those particle pairs of neighboring cells only which means that the sums in Eq. 18 are now split into partial sums corresponding to the decomposition of the simulation domain into cells. For the force $\vec{F}_i$ on particle i in cell number n one obtains a sum of the form

$$\vec{F}_i = \sum_{\substack{\text{cell } m \\ m\in\Omega(n)}} \sum_{\substack{j\in\{\text{all particles in cell } m\} \\ j\neq i}} \vec{F}_{ij}, \tag{25}$$

where $\Omega(n)$ denotes cell n itself together with all cells that are direct neighbors of cell n. The linked-cell algorithm is a simple loop over all cells of the simulation box. For each cell there is a linked list which contains a root pointer that points to the first particle in the respective cell which then points to the next particle within this particular cell, until the last particle is reached which points to zero, indicating that all particles in this cell have been considered. Then the algorithm switches to the root pointer of the next cell and the procedure is repeated until all interacting cells have been considered, cf. Fig. 3.

Assuming the average particle density in the simulation box as $\langle\rho\rangle$ then the number of particles in each one of the subcells is $\langle\rho\rangle\, r_{\text{cut}}^3$. The total number of subcells is $N/\langle\rho\rangle\, r_{\text{cut}}^3$ and

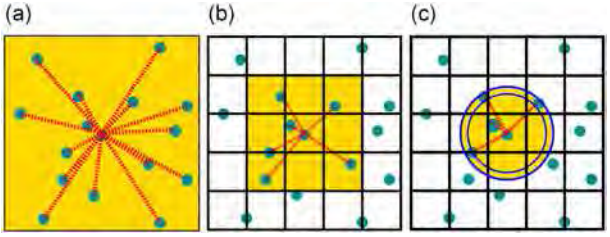

Fig. 3. MD Optimization schemes for the search of potentially interacting particles. (a) The least efficient all particle "brute force" approach with run time $\mathcal{O}(N^2)$ (b) The linked-cell algorithm which reduces the search effort to $\mathcal{O}(N)$. (c) The linked-cell algorithm combined with neighbor lists which further reduces the search effort by using a list of potentially interacting neighbor particles which can be used for several timesteps before it has to be updated. In this 2D representation, the radius of the larger circle is $r_{\text{cut}} + r_{skin}$ and the inner circle, which contains actually interacting particles, has radius r_{cut}.

the total number of neighbor cells of each subcell is 26 in a cubic lattice in three dimensions (3D). Due to Newton's third law only half of the neighbors actually need to be considered. Hence, the order to which the linked-cell algorithm reduces the search effort is given by:

$$\frac{26}{2}\left(\langle\rho\rangle\, r_{\text{cut}}^2\right)\frac{N}{\langle\rho\rangle\, r_{\text{cut}}^3} = 13(\langle\rho\rangle\, r_{\text{cut}}^3)^2 N. \tag{26}$$

For this method to function, the size of the simulation box has to be at least $3r_{\text{cut}}$, cf. Fig. 3. For simulations of dense melts with many particles, this requirement is usually met. Consequently, by this method, the search-loop effort is reduced to $\mathcal{O}(N)$, but with a pre-factor that still can be very large, depending on the density of particles $\langle\rho\rangle$ and the interaction range r_{cut}.

2.3.2 Boundary conditions

In a MD simulation only a very small number of particles can be considered. To avoid the (usually) undesired artificial effects of surface particles which are not surrounded by neighboring particles in all directions and thus are exerted to non-isotropic forces, one introduces *periodic boundary conditions*. Using this technique, one measures the "bulk" properties of the system, due to particles which are located far away from surfaces. As a rule, one uses a cubic simulation box were the particles are located. This cubic box is periodically repeated in all directions. If, during a simulation run, a particle leaves the central simulation box, then one of its image particles enters the central box from the opposite direction. Each of the image particles in the neighboring boxes moves in exactly the same way, cf. Fig. 4 for a two dimensional visualization.

The cubic box is used almost exclusively in simulations with periodic boundaries, mainly due to its simplicity, however also spherical boundary conditions have been investigated were the three-dimensional surface of the sphere induces a non-Euclidean metric. The use of periodic boundary conditions allows for the simulation of bulk properties of systems with a relatively small number of particles.

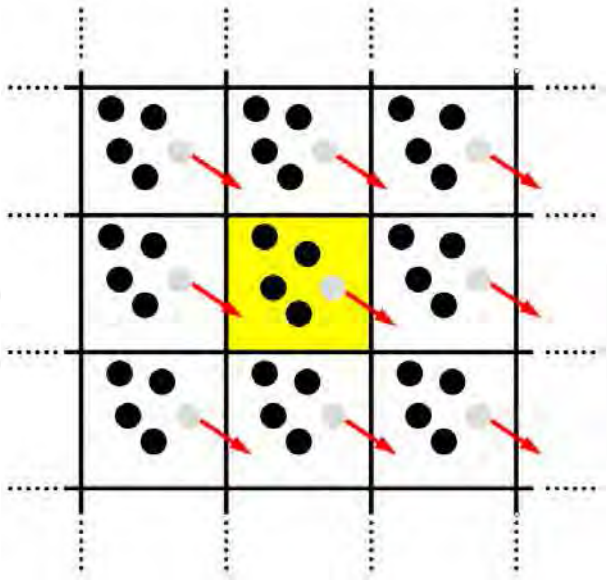

Fig. 4. Two-dimensional schematic of periodic boundary conditions. The particle trajectories in the central simulation box are copied in every direction.

2.3.3 Minimum image convention

The question whether the measured properties with a small, periodically extended system are to be regarded as representative for the modeled system depends on the specific observable that is investigated and on the range of the intermolecular potential. For a LJ potential with cut-off as in Eq. 11 no particle can interact with one of its images and thus be exposed to the artificial periodic box structure which is imposed upon the system. For long range forces, also interactions of far away particles have to be included, thus for such systems the periodic box structure is superimposed although they are actually isotropic. Therefore, one only takes into account those contributions to the energy of each one of the particles which is contributed by a particles that lies within a cut-off radius that is at the most $1/2L_B$ with boxlenth L_B. This procedure is called *minimum image convention*. Using the minimum image convention, each particle interacts with at the most $(N-1)$ particles. Particularly for ionic systems a cut-off has to be chosen such that the electro-neutrality is not violated. Otherwise, particles would start interacting with their periodic images which would render all calculations of forces and energies erroneous.

3. Complex formation of charged macromolecules

A large variety of synthetic and biological macromolecules are polyelectrolytes (Manning, 1969). The most well-known polyelectrolyte biopolymers, proteins, DNA and RNA, are responsible for functions in living systems which are incomparably more complex and diverse than the functions usually discussed for synthetic polymers present in the chemical industry. For example, polyacrylic acid is the main ingredient for diapers and dispersions of copolymers of acrylamide or methacrylamide and methacrylic acid are fundamental for

cleaning water. In retrospect, during the past 30 years, despite the tremendous interest in polyelectrolytes, unlike neutral polymers (de Gennes, 1979; Flory, 1969), the general understanding of the behavior of electrically charged macromolecules is still rather poor. The contrast between our understanding of neutral and charged polymers results form the long range nature of the electrostatic interactions which introduce new length and time scales that render an analytical treatment beyond the Debye-Hückel approximation very complicated (Barrat & Joanny, 2007; Debye & Hückel, 1923). Here, the traditional separation of scales, which allows one to understand properties in terms of simple scaling arguments, does not work in many cases. Experimentally, often a direct test of theoretical concepts is not possible due to idealizing assumptions in the theory, but also because of a lack of detailed control over the experimental system, e.g. in terms of the molecular weight. Quite recently, there has been increased interest in hydrophobic polyelectrolytes which are water soluble, covalently bonded sequences of polar (ionizable) groups and hydrophobic groups which are not (Khoklov & Khalatur, 2005). Many solution properties are known to be due to a complex interplay between short-ranged hydrophobic attraction, long-range Coulomb effects, and the entropic degrees of freedom. Hence, such polymers can be considered as highly simplified models of biologically important molecules, e.g. proteins or lipid bilayers in cell membranes. In this context, computer simulations are a very important tool for the detailed investigation of charged macromolecular systems. A comprehensive review of recent advances which have been achieved in the theoretical description and understanding of polyelectrolyte solutions can be found in (Holm et al., 2004).

3.1 Two oppositely charged macromolecules

The investigation of aggregates between oppositely charged macromolecules plays an important role in technical applications, particularly in biological systems. For example, DNA is associated with histone proteins to form the chromatin. Aggregates of DNA with cationic polymers or dendrimers are discussed in the context of their possible application as DNA vectors in gene therapies (Gössl et al., 2002; Yamasaki et al., 2001). Here, we present MD simulations of two flexible, oppositely charged polymer chains and illustrate the universal scaling properties of the resulting polyelectrolyte complexes that are formed when the chains collapse and build compact, cluster-like structures which are constrained to a small region in space (Steinauser, 1998; Winkler et al., 2002). The properties are investigated as a function of chain length N and interaction strength ξ. Starting with Eq. 5 and using $k = 1$ (cgs-system of units) the dimensionless interaction parameter

$$\xi = \xi_B k_B T / \epsilon\sigma \tag{27}$$

can be introduced, where the Bjerrum length ξ_B is given by:

$$\xi_B = e^2 / \epsilon k_B T, \tag{28}$$

where k_B is the Boltzmann constant, T is temperature, ϵ is the energy scale from the Lennard-Jones potential of Eq. 11, σ defines the length scale (size of one monomer) and e is the electronic charge.

The interaction parameter for the here presented study is chosen in the range of $\xi = 0, ..., 100$ which covers electrically neutral chains ($\xi = 0$) in good solvent as well as highly charged chain systems ($\xi = 100$). The monomers in the chains are connected by harmonic bonds

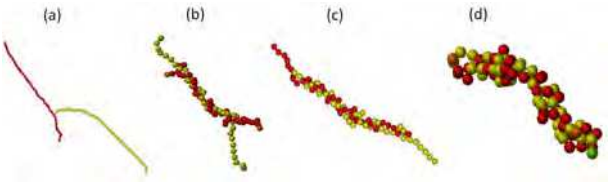

Fig. 5. Twisted, DNA-like polyelectrolyte complexes formed by electrostatic attraction of two oppositely charged linear macromolecules with $N = 40$ at different time intervals $\tau = 0$ (a), $\tau = 10500$ (b), $\tau = 60000$ (c) and $\tau = 120000$ (d), where τ is given in reduced Lennard-Jones units (Allen & Tildesly, 1991). The interaction strength is $\xi = 8$ (Steinauser, 1998; Winkler et al., 2002).

using the first term of the bonded potential of Eq. 2. The interaction with the solvent is taken into account by a stochastic force ($\vec{\Gamma}_i$) and a friction force with a damping constant χ, acting on each mass point. The equations of motion of the system are thus given by the Langevin equations

$$m\ddot{\vec{r}}_i = \vec{F}_i - \chi m\dot{\vec{r}}_i + \vec{\Gamma}_i. \tag{29}$$

The force $\vec{F}_i$ comprises the force due to the sum of the potentials of Eq. 11 with cutoff $r_{\text{cut}} = 1.5$, Eq. 6 with $k = 1$, $z_{i/j} = \pm 1$, and the first term on the right-hand side of the bonded potential in Eq. 2 with $\kappa = 5000\varepsilon/\sigma$ and bond length $l_0 = \sigma_0 = 1.0$. The stochastic force $\vec{\Gamma}_i$ is assumed to be stationary, random, and Gaussian (white noise). The electrically neutral system is placed in a cubic simulation box and periodic boundary conditions are applied for the intermolecular Lennard-Jones interaction according to Eq. 11, thereby keeping the density $\rho = N/V = 2.1 \times 10^{-7}/\sigma^3$ constant when changing the chain length N. The number of monomers N per chain was chosen as $N = 10, 20, 40, 80$ and 160 so as to cover at least one order of magnitude. For the Coulomb interaction a cutoff that is half the boxlength $r_{\text{cut}} = 1/2L_B$ was chosen. This can be done as the eventually collapsed polyelectolyte complexes which are analyzed are confined to a small region in space which is much smaller than r_{cut}. In the following we discuss exemplarily some scaling properties of charged linear macromolecules in the collapsed state. The simulations are started with two well separated and equilibrated chains in the simulation box. After turning on the Coulomb interactions with opposite charges $z_{i/j} = \pm 1$ in the monomers of both chains, the chains start to attract each other. In a first step during the aggregation process the chains start to twist around each other and form helical like structures as presented in Fig. 5. In a second step, the chains start to form a compact globular structure because of the attractive interactions between dipoles formed by oppositely charged monomers, see the snapshots in Fig. 6(a).

Figure 6(a) exhibits the universal scaling regime of R_g obtained for intermediate interaction strengths ξ and scaled by $(N-1)^{2/3}$. Here, the data of various chain lengths fall nicely on top of each other. This scaling corresponds to the scaling behavior of flexible chains in a bad solvent and is also in accordance with what was reported by Shrivastava and Muthukumar (Srivastava & Muthukumar, 1994). The change of R_g is connected with a change of the density ρ of the polyelectrolyte aggregate. However, in Fig. 6(b), which presents an example of ρ for $\xi = 4$, only a slight dependence of the density on the chain length N can be observed. ρ measures the radial monomer density with repsect to the center of mass of the total system. For longer chains, there is a plateau while for short chains there is a pronounced maximum of the density for small distances from the center of mass. While this maximum

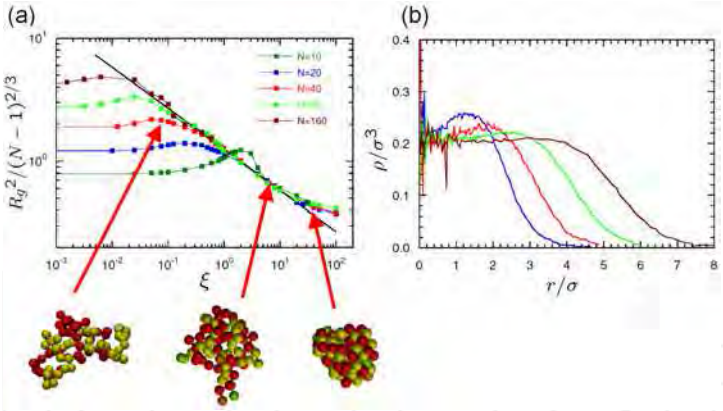

Fig. 6. (a) Radii of gyration as a function of the interaction strength ξ for various chain lengths according to (Steinhauser, 2008; Winkler et al., 2002). The radius of gyration ${R_g}^2$ which is measure for the size of a polymer chain is scaled by $(N-1)^{2/3}$, where $(N-1)$ is the number of bonds of a single chain. Also displayed are sample snapshots of the collapsed globules with $N = 40$ and interaction strengths $\xi = 0.4, 4, 40$. (b) Radial density of monomers with respect to the center of mass of a globule and interaction strength $\xi = 4$ for different chain lengths, $N = 20$ (blue), $N = 40$ (red), $N = 80$ (green) and $N = 160$ (brown).

vanished with decreasing ξ it appears also at higher interaction strengths for longer chains. Monomers on the outer part of the polyelectrolyte complex experience a stronger attraction by the inner part of the cluster than the monomers inside of it, and for smaller ξ, chains of different lengths are deformed to different degrees which leads to a chain length dependence of the density profile.

4. Equilibrium and Non-Equilibrium Molecular Dynamics (NEMD)

An understanding of the behavior of fully flexible linear polymers in dilute solutions and of dense melts has been achieved decades ago by the fundamental works of Rouse and Zimm (Zimm, 1956), as well as of Doi and Edwards (Doi & Edwards, 1986) and deGennes (de Gennes, 1979). In contrast to the well understood behavior of fully flexible linear polymers in terms of the Rouse (Prince E. Rouse, 1953) and the reptation model (de Gennes, 1979; Doi & Edwards, 1986), semiflexible polymer models have received increasing attention recently, as on the one hand they can be applied to many biopolymers like actin filaments, proteins or DNA (Käs et al., 1996; Ober, 2000) and on the other hand even for polymers considered flexible, like Polyethylene, the Rouse model fails as soon as the local chemical structure can no longer be neglected. One of the effects of this structure is a certain stiffness in the polymer chain due to the valence angles of the polymer backbone (Paul et al., 1997). Thus, semiflexible polymers are considerably more difficult to treat theoretically, as they require the fulfillment of additional constraints, such as keeping the total chain length fixed, which render these models more complex and often nonlinear. A deeper understanding of the rheological, dynamical and structural properties of semiflexible or even rod-like polymers is thus of great practical and fundamental interest.

4.1 Theoretical framework

The Kratky-Porod chain model (or worm-like chain model, WLC) (Kratky & Porod, 1949) provides a simple description of inextensible semiflexible polymers with positional fluctuations that are not purely entropic but governed by their bending energy Φ_{bend} and characterized e.g. by their persistence length L_p. The corresponding elastic energy

$$\Phi_{\text{bend}} = \frac{\kappa}{2} \int_0^L ds \left(\frac{\partial^2 \mathbf{r}}{\partial s^2} \right)^2 \tag{30}$$

of the inextensible chain of length L depends on the local curvature of the chain contour s, where $\vec{r}(s)$ is the position vector of a mass point (a monomer) on the chain and κ is a constant (Doi & Edwards, 1986).

Harris and Hearst formulated an equation of motion for the WLC model by applying Hamilton's principle with the constraint that the second moment of the total chain length be fixed and obtained the following expressions for the bending $\vec{F}_{\text{bend}}$ and tension forces $\vec{F}_{\text{tens}}$

$$\vec{F}_{\text{bend}} = \mu \frac{\partial^4 \vec{r}}{\partial s^4}, \tag{31}$$

$$\vec{F}_{\text{tens}} = \omega \frac{\partial^2 \vec{r}}{\partial s^2}. \tag{32}$$

Applying this result to elastic light scattering, this model yields correct results in the flexible coil limit (Harris & Hearst, 1966), but it fails at high stiffness, where it deviates from the solution obtained for rigid rods (Harris & Hearst, 1967).

A different model was proposed by Soda (Soda, 1973), where the segmental tension forces are modeled by stiff harmonic springs. This approach avoids large fluctuations in the contour length but has the disadvantage that an analytic treatment of the model is possible only for few limiting cases. Under the assumption that the longitudinal tension relaxes quickly, the bending dynamics can be investigated using a normal mode analysis (Aragón & Pecora, 1985; Soda, 1991). However, this approach cannot account for the flexible chain behavior which is observed on large length scales in the case $L_p \ll L$.

Winkler, Harnau and Reineker (Harnau et al., 1996; R.G. Winkler, 1994) considered a Gaussian chain model and used a Langevin equation similar to the equation employed by Harris and Hearst, but introduced separate Lagrangian multipliers for the end points of the chain, thus avoiding the problems of the Harris and Hearst equation in the rod-like limit. Thus, the equation used in (Harris & Hearst, 1966) is contained in the model used by Winkler, Harnau and Reineker and can be regained by setting all Lagrangian multipliers equal along the chain contour and at the end points. The expansion of the position vector $\vec{r}(s)$ in normal coordinates in the approach used in (R.G. Winkler, 1994) and resolving the obtained equations for the relaxation times τ_p or the normal mode amplitudes $X_p(t)$ leads to a set of transcendental equations, the solution of which cannot be given in closed form. For some limiting cases, Harnau, Winkler and Reineker showed the agreement of the approximate solution of the transcendental equations with atomistic simulation results of a n-$C_{100}H_{202}$ polymer melt (Harnau et al., 1999) that were performed by Paul, Yoon and Smith (Paul et al., 1997).

In contrast to fully flexible polymers, the modeling of *semiflexible* and *stiff* macromolecules has received recent attention, because such models can be successfully applied to biopolymers such as proteins, DNA, actin filaments or rodlike viruses (Bustamante et al., 1994; Ober, 2000). Biopolymers are wormlike chains with persistence lengths l_p (or Kuhn segment lengths l_K) comparable to or larger than their contour length L and their rigidity and relaxation behavior are essential for their biological functions.

4.2 Modeling and simulation of semiflexible macromolecules

Molecular Dynamics simulations were performed using the MD simulation package "MD-Cube", which was originally developed by Steinhauser (Steinhauser, 2005). A coarse-grained bead-spring model with excluded volume interactions as a model for dilute solutions of polymers in solvents of varying quality, respectively for polymer melts, is employed (Steinhauser, 2008; Steinhauser & et. al., 2005). A compiler switch allows for turning on and off the interaction between different chains. Thus, one can easily switch the type of simulation from single polymers in solvent to polymer melts. The excluded volume for each monomer is taken into account through the potential of Eq. 11.

Neighboring mass points along the chains are connected by harmonic bonds with the following potential for the bonded interactions

$$\Phi_{\text{bonded}}(r) = \frac{K}{2}(r - d_0)^2 \,, \tag{33}$$

which is often used in polymer simulations of charged, DNA-like biopolymers, see e.g. (Steinauser, 1998; Winkler et al., 2002). Note, that the potential in Eq. 33 corresponds to the first term on the right-hand side of Eq. 2. In order to keep fluctuations of the bond lengths and thus the fluctuations of the overall chain length L small (below 1%), a large value for the force constant $K = 10000\varepsilon/\sigma^2$ is chosen, where ε and σ are parameters of the truncated LJ-potential in Eq. 11. The average bondlength d_0 is taken to be 0.97σ which is the equilibrium distance of a potential that is composed of the FENE (Finite Extensible Non-Linear Elastic) potential – which is frequently employed in polymer simulations (Steinhauser, 2005) – and the truncated LJ-potential of Eq. 11. In combination with the LJ-potential this particle distance keeps the chain segments from artificially crossing each other (Steinhauser, 2008). The FENE potential exhibits very large fluctuations of bond lengths which are unrealistic for the investigation of semiflexible or stiff polymers. This is the reason for choosing the simple harmonic potential in Eq. 33). It is noted, that in principle the exact analytic form of the bonded potential when using a coarse-grained polymer model is actually irrelevant as long as it ensures that the the basic properties of polymers are modeled correctly such as the specific connectivity of monomers in a chain, the non-crossability of monomer segments (topological constraints), or the flexibility/stiffness of a chain. Thus, very often, a simple potential that can be quickly calculated in a numerical approach is used.

The stiffness, i.e. the bending rigidity of the chains composed of N mass points, is introduced into the coarse-grained model by the following bending potential

$$\Phi_{\text{bend}} = \frac{\kappa}{2} \sum_{i=1}^{N-1} (\vec{u}_{i+1} - \vec{u}_i)^2 = \kappa \sum_{i=1}^{N-1} (1 - \vec{u}_{i+1} \cdot \vec{u}_i) \,, \tag{34}$$

where $\vec{u}$ is the unit bond vector $\vec{u}_i = (\vec{r}_{i+1} - \vec{r}_i)/\mid \vec{r}_{i+1} - \vec{r}_i \mid$ connecting consecutive monomers, and $\vec{r}_i$ is the position vector to the i-th monomer. The total force acting on monomer i is thus given by

$$\vec{F}_i = -\partial/\partial\vec{r}_i \Phi_{\text{total}} = -\partial/\partial\vec{r}_i \left(\Phi_{\text{LJ}}^{\text{cut}} + \Phi_{\text{bonded}} + \Phi_{\text{bend}} \right) . \tag{35}$$

Assuming a NVT ensemble at temperature $k_B T = 1\varepsilon$, the trajectories of all particles $i = (1, ..., N)$ are generated by integrating the stochastic equations of motion

$$\frac{d^2\vec{r}_i}{dt^2} = -\xi \frac{d\vec{r}_i}{dt} + \frac{1}{m}\vec{F}_i + \frac{1}{m}\vec{F}_i^S , \tag{36}$$

with a particle friction coefficient ξ and a Gaussian stochastic force $\vec{F}_i^S$ that satisfies

$$< \vec{F}_i^S(t) >= 0 , \tag{37}$$

and the fluctuation-dissipation-theorem

$$< F_i^S(t) F_j^S(t') >= 2kT\xi\delta_{ij}\delta(t - t') . \tag{38}$$

The equations of motion are integrated using the Brownian dynamics algorithm proposed by van Gunsteren and Berendsen for a canonical ensemble (van Gunsteren & Berendsen, 1982) which – for vanishing particle friction ξ – changes into the velocity Verlet algorithm for a microcanonical ensemble. The algorithm is used with a constant timestep of $\Delta t = 5 \times 10^{-3}\tau$, where τ is the time unit of the simulation.

4.2.1 Results

The crossover scaling from coil-like, flexible structures on large length scales to stretched conformations at smaller scales can be seen in the scaling of the structure function $S(q)$ when performing simulations with different values of k_θ (Steinhauser, Schneider & Blumen, 2009).

In Fig. 7(a) the structure functions of the simulated linear polymer chains of length $N = 700$ are displayed for different persistence lengths. The chains show a scaling according to q^ν. The stiffest chains exhibit a q^{-1}–scaling which is characteristic for stiff rods. The dotted and dashed lines display the expected theoretical scaling behavior.

Thus, by varying parameter k_θ, the whole range of bending stiffness of chains from fully flexible chains to stiff rods can be covered. The range of q–values for which the crossover from flexible to semiflexible and stiff occurs, shifts to smaller q–values with increasing stiffness k_θ of the chains. The scaling plot in Fig. 7(b) shows that the transition occurs for $q \approx 1/l_K$, i.e. on a length scale of the order of the statistical Kuhn length. In essence, only the fully flexible chains (red data points) exhibit a deviation from the master curve on large length scales (i.e. small q–values), which corresponds to their different global structure compared with semi-flexible macromolecules. Examples for snapshots of stiff and semiflexible chains are displayed in Fig. 8.

For a theoretical treatment, following Doi and Edwards (Doi & Edwards, 1986), we expand the position vector $\vec{r}(s,t)$ of a polymer chain, parameterized with time t and contour length s

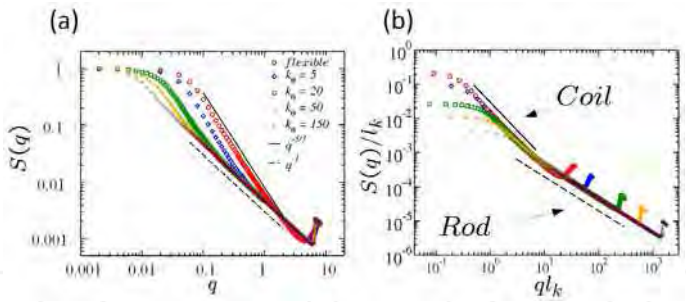

Fig. 7. (a) Structure function $S(q)$ of single linear chains with $N = 700$ and varying stiffness k_θ. The scaling regimes (fully flexible and stiff rod) are indicated by a straight and dashed line, respectively. (b) Scaling plot of $S(q)/l_K$ versus $q \cdot l_K$ using the statistical segment length l_K, adapted from (Steinhauser, Schneider & Blumen, 2009).

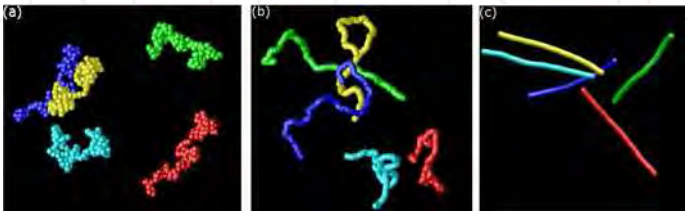

Fig. 8. Simulation snapshots of (a) flexible chains ($k_\theta = 0$), (b) semiflexible chains ($k_\theta = 20$), (c) stiff, rod-like chains ($k_\theta = 50$).

in normal modes $\vec{X}_p(t)$ as follows:

$$\vec{r}(s,t) = \vec{X}_0(t) + 2\sum_{p=1}^{\infty}(t)\cos\left(\frac{p\pi}{L}s\right). \tag{39}$$

Resolving Eq. 39 for the normal modes and inserting the result into the Langevin equations of motion for $\vec{r}(s,t)$ one obtains after some algebraic manipulations for the relaxation time τ_p

$$\tau_p = \frac{3k_BT\pi^2p^2}{2L^2\xi}\left[\frac{1}{L_p} + \frac{L_p\pi^2}{NL}p^2\right], \tag{40}$$

which can be interpreted physically as arising from contributions due to an entropic force term $\propto p^2$ and a bending force term $\propto p^4$. In Fig. 9 we show that our simulation results for semiflexible chains scale according to Eq. 40.

Figure 10 exhibits the results of a NEMD step-shear simulation, from which the shear modulus $G(t)$ has been determined. The NEMD scheme produces the same results for the shear modulus $G(t)$ as conventional methods at equilibrium, which are based on the Green-Kubo equation.

Finally, in Fig. 11 we illustrate our step-shear simulation scheme for polymer melts with two corresponding NEMD simulation snapshots.

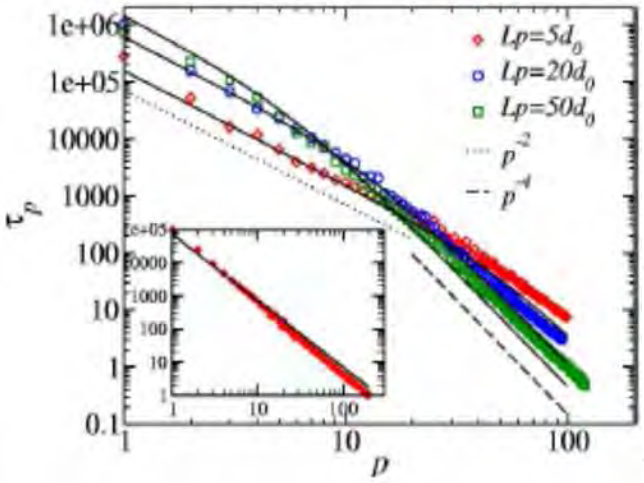

Fig. 9. Scaling of relaxation time τ_p for semiflexible chains ($N = 700$) with different L_p. The dotted and dashed lines show the scaling behavior according to Eq. 40. The inset shows τ_p of our simulated flexible chains compared with the Rouse model.

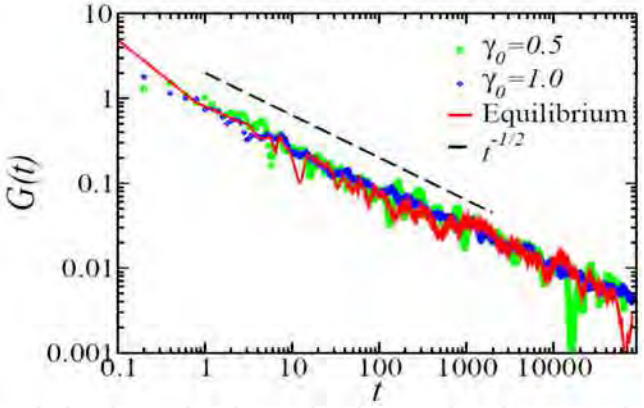

Fig. 10. Shear modulus $G(t)$ obtained from NEMD simulations compared with conventional (red line) equilibrium methods. The dashed line displays the expected Rouse scaling behavior and γ_0 displays the respective shear rates of the systems.

5. Shock wave failure of granular materials

In the following we discuss a recently proposed concurrent multiscale approach for the simulation of failure and cracks in brittle materials which is based on mesoscopic particle dynamics, the Discrete Element Method (DEM), but which allows for simulating macroscopic properties of solids by fitting only a few model parameters (Steinhauser, Grass, Strassburger & Blumen, 2009).

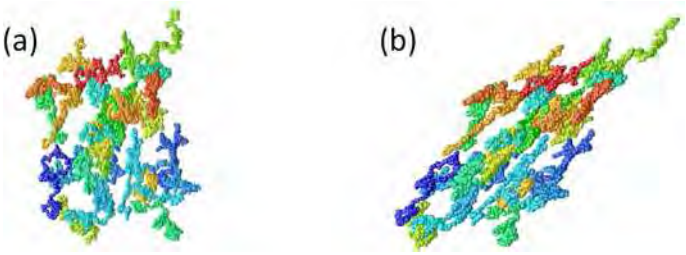

Fig. 11. Non-equilibrium shear-simulation of $N = 100$ polymer chains with $N = 100$ particles each (a) before and (b) after shearing the system. For reasons of clarity only 30 different chains of the system are displayed.

5.1 Introduction: Multiscale modeling of granular materials using MD

Instead of trying to reproduce the geometrical shape of grains on the microscale as seen in two-dimensional (2D) micrographs, in the proposed approach one models the macroscopic solid state with soft particles, which, in the initial configuration, are allowed to overlap, cf. Fig. 12(a). The overall system configuration, see Fig. 12(b), can be visualized as a network of links that connect the centers of overlapping particles, cf. Fig. 12(c).

The degree of particle overlap in the model is a measure of the force that is needed to detach particles from each other. The force is imposed on the particles by elastic springs. This simple model can easily be extended to incorporate irreversible changes of state such as plastic flow in metals on the macro scale. However, for brittle materials, where catastrophic failure occurs after a short elastic strain, in general, plastic flow behavior can be completely neglected. Additionally, a failure threshold is introduced for both, extension and compression of the springs that connect the initial particle network. By adjusting only two model parameters for the strain part of the potential, the correct stress-strain relationship of a specific brittle material as observed in (macroscopic) experiments can be obtained. The model is then applied to other types of external loading, e.g. shear and high-speed impact, with no further model adjustments, and the results are compared with experiments performed at EMI.

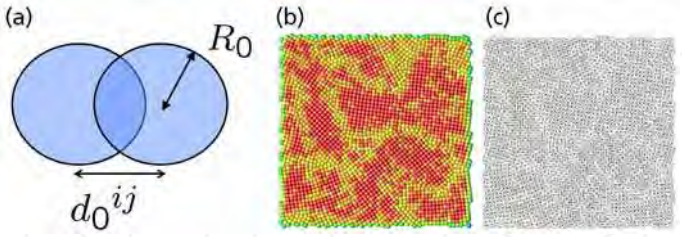

Fig. 12. The particle model as suggested in (Steinhauser, Grass, Strassburger & Blumen, 2009). (a) Overlapping particles with radii R_0 and the initial (randomly generated) degree of overlap indicated by $d_0{}^{ij}$. Here, only two particles are displayed. In the model the number of overlapping particles is unlimited and *each* individual particle pair contributes to the overall pressure and tensile strength of the solid. (b) Sample initial configuration of overlapping particles $(N = 2500)$ with the color code displaying the coordination number: red (8), yellow (6), and green (4). (c) The same system displayed as an unordered network.

5.2 Model potentials

The main features of a coarse-grained model in the spirit of Occam's razor with only few parameters, are the repulsive forces which determine the materials resistance against pressure and the cohesive forces that keep the material together. A material resistance against pressure load is introduced by a simple Lennard Jones type repulsive potential Φ_{rep}^{ij} which acts on every pair of particles $\{ij\}$ once the degree of overlap d^{ij} decreases compared to the initial overlap ${d_0}^{ij}$:

$$\phi_{rep}^{ij}\left(\gamma, d^{ij}\right) = \begin{cases} \gamma {R_0}^3 \left(\left(\frac{{d_0}^{ij}}{d^{ij}}\right)^{12} - 2\left(\frac{{d_0}^{ij}}{d^{ij}}\right)^{6} + 1 \right) & : \quad 0 < d^{ij} < {d_0}^{ij} \\ 0 & : \quad d^{ij} \geq {d_0}^{ij} \end{cases} . \tag{41}$$

Parameter γ scales the energy density of the potential and prefactor ${R_0}^3$ ensures the correct scaling behavior of the calculated total stress $\Sigma_{ij}\sigma^{ij} = \Sigma_{ij}F^{ij}/A$ which, as a result, is independent of N. Figure 13 shows that systems with all parameters kept constant, but only N varied, lead to the same slope (Young's modulus) in a stress-strain diagram. In Eq. 41 R_0 is the constant radius of the particles, $d^{ij} = d^{ij}(t)$ is the instantaneous mutual distance of each interacting pairs $\{ij\}$ of particles, and ${d_0}^{ij} = d^{ij}(t=0)$ is the initial separation which the pair $\{ij\}$ had in the starting configuration. Every single pair $\{ij\}$ of overlapping particles is associated with a different initial separation ${d_0}^{ij}$ and hence with a different force. The minimum of each individual particle pair $\{ij\}$ is chosen such that the body is force-free at the start of the simulation.

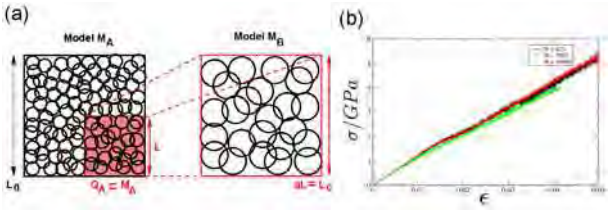

Fig. 13. (a) Schematic of the intrinsic scaling property of the proposed material model. Here, only the 2D case is shown for simplicity. The original system (Model M_a) with edge length L_0 and particle radii R_0 is downscaled by a factor of $1/a$ into the subsystem Q_A of M_A (shaded area) with edge length L, while the particle radii are upscaled by factor a. As a result, model M_B of size $aL = L_0$ is obtained containing much fewer particles, but representing the same macroscopic solid, since the stress-strain relation (and hence, Young's modulus E) upon uni-axial tensile load is the same in both models. (b) Young's modulus E of systems with different number of particles N in a stress-strain ($\sigma - \varepsilon$) diagram. In essence, E is indeed independent of N.

When the material is put under a low tension the small deviations of particle positions from equilibrium will vanish as soon as the external force is released. Each individual pair of overlapping particles can thus be visualized as being connected by a spring, the equilibrium length of which equals the initial distance ${d_0}^{ij}$. This property is expressed in the cohesive potential by the following equation:

$$\Phi_{coh}^{ij}\left(\lambda, d^{ij}\right) = \lambda R_0 \left(d^{ij} - {d_0}^{ij}\right)^2, \; d^{ij} > 0. \tag{42}$$

In this equation, λ (which has dimension [energy/length]) determines the strength of the potential and prefactor R_0 again ensures a proper intrinsic scaling behavior of the material response. The total potential is the following sum:

$$\Phi_{tot} = \Sigma_{ij} \left(\phi_{rep}^{ij} + \phi_{coh}^{ij} \right). \tag{43}$$

The repulsive part of Φ_{tot} acts only on particle pairs that are closer together than their mutual initial distance ${d_0}^{ij}$, whereas the harmonic potential Φ_{coh} either acts repulsively or cohesively, depending on the actual distance d^{ij}. Failure is included in the model by introducing two breaking thresholds for the springs with respect to compressive and to tensile failure, respectively. If either of these thresholds is exceeded, the respective spring is considered to be broken and is removed from the system. A tensile failure criterium is reached when the overlap between two particles vanishes, i.e. when:

$$d^{ij} > (2R_0). \tag{44}$$

Failure under pressure load occurs when the actual mutual particle distance is less by a factor α (with $\alpha \in (0,1)$) than the initial mutual particle distance, i.e. when

$$d^{ij} < \alpha \cdot {d_0}^{ij}. \tag{45}$$

Particle pairs without a spring after pressure or tensile failure still interact via the repulsive potential and cannot move through each other.

An appealing feature of this model, as opposed to many other material models used for the description of brittle materials, see e.g. (Cundall & Strack, 1979; Leszczynski, 2003; Walton & Braun, 1986), is its simplicity. The proposed model has a total of only three free parameters: γ and λ for the interaction potentials and α for failure. These model parameters can be adjusted to mimic the behavior of specific materials.

5.3 Shock wave simulations and comparison with experiments

Finally, in Fig. 14, non-equilibrium MD simulation (NEMD) results for systems with varying shock impact velocities are presented and compared with high-speed impact experiments performed at EMI with different ceramic materials (Al_2O_3 and SiC) in the so-called edge-on-impact (EOI) configuration. These oxide and non-oxide ceramics represent two major classes of ceramics that have many important applications. The impactor hits the target at the left edge. This leads to a local compression of the particles in the impact area.

The top series of snapshots in Fig. 14(a) shows the propagation of a shock wave through the material. The shape of the shock front and also the distance traveled by it correspond very well to the high-speed photographs in the middle of Fig. 14(a). These snapshots were taken at comparable times after the impact had occurred in the experiment and in the simulation, respectively. In the experiments which are used for comparison, specimens of dimensions $(100 \times 100 \times 10) mm$ were impacted by a cylindrical blunt steel projectile of length $23\,mm$, mass $m = 126\,g$ and a diameter of $29.96\,mm$ (Steinhauser et al., 2006). After a reflection of the pressure wave at the free end of the material sample, and its propagation back into the material, the energy stored in the shock wave front finally disperses in the material. One can study in great detail the physics of shock waves traversing the material and easily

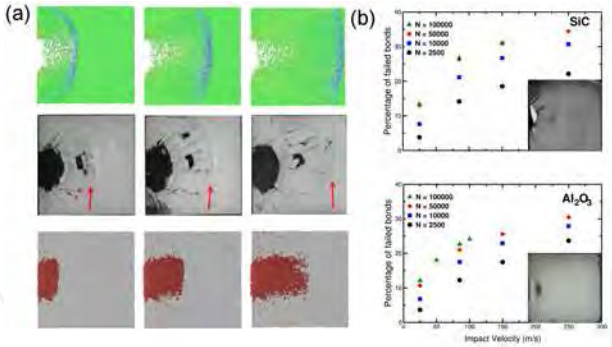

Fig. 14. Results of a simulation of the edge-on-impact (EOI) geometry, except this time, the whole macroscopic geometry of the experiment can be simulated while still including a microscopic resolution of the system. The impactor is not modeled explicitly, but rather its energy is transformed into kinetic energy of the particle bonds at the impact site. (a) Top row: A pressure wave propagates through the material and is reflected at the free end as a tensile wave (not shown). Middle row: The actual EOI experiment with a SiC specimen. The time interval between the high-speed photographs is comparable with the simulation snapshots above. The red arrows indicate the propagating shock wave front. Bottom row: The same simulation run but this time only the occurring damage in the material with respect to the number of broken bonds is shown. (b) Number of broken bonds displayed for different system sizes N, showing the convergence of the numerical scheme. Simulation parameters $(\alpha, \gamma, \lambda)$ are chosen such that the correct stress-strain relations of two different materials (Al_2O_3 and SiC) are recovered in the simulation of uniaxial tensile load. The insets show high-speed photographs of SiC and Al_2O_3, respectively, $4\mu s$ after impact.

identify strained or compressed regions by plotting the potential energies of the individual pair bonds. Also failure in the material can conveniently be visualized by plotting only the failed bonds as a function of time, cf. the bottom series of snapshots in Fig. 14(a). A simple measure of the degree of damage is the number of broken bonds with respect to the their total initial number. This quantity is calculated from impact simulations of Al_2O_3 and SiC, after previously adjusting the simulation parameters γ, λ and α accordingly. Figure 14(b) exhibits the results of this analysis. For all impact speeds the damage in the SiC-model is consistently larger than in the one for Al_2O_3 which is also seen in the experiments.

The impactor is not modeled explicitly, but rather its total kinetic energy is transformed into kinetic energy of the particles in the impact region. Irreversible deformations of the particles such as plasticity or heat are not considered in the model, i.e. energy is only removed from the system by broken bonds. Therefore, the development of damage in the material is slightly overestimated.

6. Conclusions

In summary, we presented an introduction into the molecular dynamics method, discussing the choice of potentials and fundamental algorithms for the implementation of the MD method. We then discussed proto-typical applications of MD, namely the collapse of two oppositely charged macromolecules (polyelectrolytes) and the simulation of semiflexible

bio-macromolecules[6]. We demonstrated how semiflexibility, or stiffness of polymers can be included in the potentials describing the interactions of particles. We finally showed a somewhat unusual application of MD in the field of solid state physics where we modeled the brittle failure behavior of a typical ceramic and simulated explicitly the set-up of corresponding high-speed impact experiments. We showed that the discussed multiscale particle model reproduces the macroscopic physics of shock wave propagation in brittle materials very well while at the same time allowing for a resolution of the material on the micro scale and avoiding typical problems (large element distortions, element-size dependent results) of Finite Elements, which constitutes a different type of discretization for simulation problems that are closely connected with macroscopic experiments. The observed failure and crack pattern in impact MD simulations can be attributed to the random initial distribution of particle overlaps which generates differences in the local strength of the material. By generating many realizations of systems with different random initial overlap distributions of particles, the average values obtained from these many simulations lead to the presented fairly accurate results when compared with experimental high-speed impact studies.

7. References

Allen, M. & Tildesly, D. (1991). *Computer Simulation of Liquids*, Oxford University Press.

Aragón, S. & Pecora, R. (1985). Dynamics of wormlike chains, *Macromolecules* 18: 1868–1875.

Barrat, J.-L. & Joanny, F. (2007). Theory of Polyelectrolyte Solutions, *Adv. Chem. Phys.* 94: 1–66.

Buckingham, R. (1938). The Classical Equation of State of Gaseous Helium, Neon and Argon, *Proc. Roy. Soc* A106: 264.

Bustamante, C., Marko, J., Siggia, E. & Smith, S. (1994). Entropic Elasticity of Lambda-Phage DNA, *Science* 265: 1599–1600.

Cundall, P. & Strack, O. (1979). A Discrete Numerical Model for Granular Assemblies, *Geotechnique* 29: 47–65.

de Gennes, P. G. (1979). *Scaling Concepts in Polymer Physics*, Cornell University Press, Ithaca, London.

Debye, P. & Hückel, E. (1923). The Theory of Electrolytes. I. Lowering of Freezing Point and Related Phenomena, *Physikalische Zeitschrift* 24: 185–206.

Doi, M. & Edwards, S. (1986). *The Theory of Polymer Dynamics*, Clarendon Press, Oxford.

Feller, S. (2000). An Improved Empirical Potential Energy Function for Molecular Simulations of Phospholipids, *J. Phys. Chem. B* 104: 7510–7515.

Flory, P. (1969). *Statistical Mechanics of Chain Molecules*, Wiley, New York.

Gössl, I., Shu, L., Schlüter, A. & Rabe, J. (2002). Complexes of DNA and positively charged dendronized polymers, *J. Am. Chem. Soc.* 124: 6860.

Haberland, R., Fritsche, S., Peinel, G. & Heinzinger, K. (1995). *Molekulardynamik - Grundlagen und Anwendungen*, Friedrich VIeweg & Sohn Verlagsgesellschaft mbH, Braunschweig, Wiesbaden.

Haile, J. (1992). *Molecular dynamics simulation: Elementary Methods*, Wiley, New York.

Harnau, L., Winkler, R. & Reineker, P. (1996). Dynamic structure factor of semiflexible macromolecules in dilute solution, *J. Chem. Phys.* 104(16): 6255–6258.

[6] Semiflexibility is a characteristic feature of bio-macromolecules such as DNA, F-actin, intermediate filaments or microtubuli which are present in the cytoplasm of cells.

Harnau, L., WInkler, R. & Reineker, P. (1999). Comment on "Chain Motion in an unentangled polyethylene melt: A critical test of the Rouse model by molecular dynamics simulations anhd neutron spin echo spectroscopy, *Phys. Rev. Lett.* 82: 2408.

Harris, R. A. & Hearst, J. E. (1966). On polymer dynamics, *J. Chem. Phys.* 44: 2595–2602.

Harris, R. & Hearst, J. (1967). On Polymer Dynamics. III. Elastic Light Scattering, *J. Chem. Phys.* 46: 398.

Hockney, R. (1970). The Potential Calculation And Some Applications, *Methods Comp. Phys.* 9: 136–211.

Holm, C., Joanny, J.-P., Kremer, K., Netz, R., Reineker, P., Seidel, C., Vilgis, T. A. & Winkler, R. G. (2004). Polyelectrolyte Theory, *Adv. Polym. Sci.* 166: 67–111.

Käs, J., Strey, H., Tang, J., Finger, D., Ezzell, R., Sackmann, E. & Janmey, P. (1996). F-actin, a model polymer for semiflexible chains in dilute, semidilute, and liquid crystalline solutions, *Biophys. J.* 70: 609–625.

Khoklov, A. R. & Khalatur, P. G. (2005). Solution Properties of Charged Hydrophobic/Hydrophilic Copolymers, *Curr. Opin. Colloid Interface Sci.* 10: 22–29.

Kratky, O. & Porod, G. (1949). Röntgenuntersuchung gelöster Fadenmoleküle, *Rec. Trv. Chim* 68: 1106–1115.

Leszczynski, J. S. (2003). A Discrete Model of a Two-Particle Contact Applied to Cohesive Granular Materials, *Granular Matter* 5: 91.

Manning, G. (1969). Limiting Laws and Counterion Condensation in Polyelectrolyte Solutions I. Colligative Properties, *J. Chem. Phys.* 51: 924–933.

Ober, C. (2000). Shape Persisitence of Synthetic Polymers, *Science* 288(5465): 448–449.

Paul, W., Smith, G. & Yoon, D. (1997). Static and dynamic properties of a n - $C_{100}H_{202}$ melt from molecular dynamics simulations, *Macromolecules* 30: 7772–7780.

Prince E. Rouse, J. (1953). A Theory of the Linear Viscoelastic Properties of Dilute Solutions of Coiling Polymers, *J. Chem. Phys.* 21: 1281–1286.

R.G. Winkler, P. Reineker, L. H. (1994). Models and equilibrium properties of stiff molecular chains, *J. Chem. Phys.* 101(9): 8119–8129.

Schlenkrich, M., Brinckmann, J., MacKerell, A. & Karplus, M. (1996). *Empirical Potential Energy Function for Phospholipids: Criteria for Parameter Optimization and Applications*, Birkhäuser, Boston.

Shih, A. Y., Arkhipov, A., Freddolino, P. L. & Schulten, K. (2006). Coarse Grained Protein-Lipid Model With Application to Lipoprotein Particles, *J. Phys. Chem. B* 110: 3674–3684.

Siu, S. W., Vácha, R., Jungwirth, P. & Böckmann, R. A. (2008). Biomolecular Simulations of Membranes: Physical Properties from Different Force Fields, *J. Chem. Phys.* 125: 125103.

Soda, K. (1973). Dynamics of Stiff Chains. I. Equation of Motion, *J. Phys. Soc. Jpn.* 35: 866–870.

Soda, K. (1991). Differences in thermal conformation fluctuation between two models for semiflexible chains, *J. Chem. Phys.* 95: 9337–9347.

Srivastava, D. & Muthukumar, M. (1994). Interpenetration Of Interacting Polyelectrolytes, *Macromolecules* 27: 1461–1465.

Steinauser, M. O. (1998). *Molekulardynamik-Simulationen von Polyelectrolyten unterschiedlicher Ladungsdichte: Polyelektrolyt-Komplexbildung*, Master's thesis, University of Ulm, Germany.

Steinhauser, M. O. (2005). A Molecular Dynamics Study on Universal Properties of Polymer Chains in Different Solvent Qualitites. Part I: A Review of Linear Chain Properties, *J. Chem. Phys.* 122: 094901.

Steinhauser, M. O. (2008). *Computational Multiscale Modeling of Solids and Fluids – Theory and Applications*, Springer, Berlin, Heidelberg, New York.

Steinhauser, M. O. (2012). *Computer Simulation in Physics and Engineering*, de Gruyter. To be published in October 2012, ISBN 978-3-11-025590-4.

Steinhauser, M. O. & et. al. (2005). MAVO MMM-Tools: Entwicklung von durchgängigen Multiskalen Material Modellierungen, *Technical Report 17/05*, Fraunhofer Ernst-Mach-Institute (EMI), Freiburg, Eckerstrasse 4, 79104 Freiburg i. Br., Germany.

Steinhauser, M. O., Grass, K., Strassburger, E. & Blumen, A. (2009). Impact Failure of Granular Materials – Non-Equilibrium Multiscale Simulations and High-Speed Experiments, *International Journal of Plasticity* 25: 161–182.

Steinhauser, M. O., Grass, K., Thoma, K. & Blumen, A. (2006). A Nonequilibrium Molecular Dynamics Study on Shock Waves, *Europhys. Lett.* 73: 62.

Steinhauser, M. O., Schneider, J. & Blumen, A. (2009). Simulating Dynamic Crossover Behavior of Semiflexible Linear Polymers in Solution and in the Melt, *J. Chem. Phys.* 130: 164902.

van Gunsteren, W. & Berendsen, H. (1982). Algorithms for Brownian Dynamics, *Molec. Phys.* 45: 637.

Walton, O. R. & Braun, R. L. (1986). Viscosity, Granular-Temperature, and Stress Calculation for Shearing Assemblies of Inelastic, Frictional Disks, *J. Rheol.* 39(5): 949.

Winkler, R. G., Steinhauser, M. O. & Reineker, P. (2002). Complex Formation in Systems of Oppositely Charged Polyelectrolytes: A Molecular Dyamics Simulation Study, *Phys. Rev. E* 66: 021802.

Yamasaki, Y., Teramoto, Y. & Yoshikawa, K. (2001). Disappearance Of The Negative Charge in Giant DNA With A Folding transition, *Biophys. J.* 80: 2823Ű2832.

Zimm, B. H. (1956). Dynamics of Polymer Molecules in Dilute Solution: Viscoelasticity, Flow Birefringence and Dielectric Loss, *J. Chem. Phys.* 24: 269–278.